Rare earth element fractionation in heterogenite (CoOOH): Implication for cobalt oxidized ore in the Katanga Copperbelt (Democratic Republic of Congo)

Sophie Decree, Olivier Pourret, Jean-Marc Baele

Rare earth element fractionation in heterogenite (CoOOH): Implication for cobalt oxidized ore in the Katanga Copperbelt (Democratic Republic of Congo)

Sophie Decrée[a,b], Olivier Pourret[c] and Jean-Marc Baele[d]

[a] Royal Belgian Institute of Natural Sciences, Geological Survey of Belgium, Rue Vautier 13, B-1000 Brussels (Belgium). E-mail: sophie.decree@naturalsciences.be; phone number: +32.2.627.43.23

[b]Royal Museum for Central Africa, 3080 Tervuren, Belgium

[c]HydrISE, LaSalle Beauvais, 60026 Beauvais cedex, France. E-mail : olivier.pourret@lasalle-beauvais.fr

[d] University of Mons (Belgium). E-mail: jean-marc.baele@umons.ac.be

Abstract

Heterogenite (CoOOH) is the most abundant cobalt oxide mineral in the Katanga Copperbelt, which hosts around half of the world's known reserves of mineable cobalt. Heterogenite formed by the oxidation of Co-sulfides and accumulated as residual deposits during a Pliocene weathering event. Bulk analysis samples of oxidized cobalt ore samples containing with variable heterogenite concentration display two rare earth element (REE) patterns: (i) Type 1 is enriched in middle REE, with a negative cerium anomaly and a relatively low REE content; (ii) Type 2 is variably enriched in light REE (LREE), without a cerium anomaly and

with higher REE content. However, *in situ* LA-ICP-MS reveals that the Type 2 patterns are due to the mixing of heterogenite with a LREE-rich mineral.

Weathering processes leading to heterogenite formation mainly consist of water-rock interactions at high Co activity, in the near-surface environment. These result in the formation of a lateritic deposit. Heterogenite precipitates at near-neutral pH conditions together with manganese oxides. REE are mainly fractionated between these Co-and Mn-oxide minerals. In the deeper part of the oxidized profile, cobalt activity decreases and the heterogenite stability field shifts to alkaline pH conditions due to the dissolution of dolostone in the bedrock. In such an alkaline environment, REE speciation is mainly driven by carbonate complexation/precipitation. This environment would be favorable for the formation of REE-rich carbonate which is intimately associated with heterogenite (LREE-rich Type 2 patterns).

The combined whole-rock and in situ geochemical analyses presented here clearly help (1) to distinguish the REE signature of the Co oxidized ore (mineral paragenesis comprizing heterogenite) and of heterogenite itself, and subsequently (2) to highlight two different chemical environments for the formation of heterogenite in supergene ores. This study therefore improves the understanding of REE behaviour and metal mobility in near-surface environments, and more particularly in environments where the supergene ores form. In the future, the approach developped here can be applied to other Co-Ni-Mn lateritic deposits such as those in New-Caledonia and Cameroon.

Keywords: Cobalt, lanthanide, Katanga, Democratic Republic of Congo, Manganese oxide, LA-ICP-MS

1. Introduction

The Katanga Copperbelt is situated in the southeastern Democratic Republic of Congo, which is part of the Lufilian fold-and-thrust belt and hosts ~45% of the world's known reserves of mineable cobalt (3.4 Mt Co metal content; USGS, 2014).

Heterogenite (CoOOH) is the most abundant cobalt oxide in the Copperbelt. Previous works on the Katanga heterogenite (Hey, 1962; Deliens, 1974; Deliens and Goethals, 1973; Gauthier and Deliens, 1999; Burlet et al., 2011; Vanbrabant, 2013) distinguished two sub-types of heterogenite: (i) rhombohedral heterogenite 3R is the most abundant variety (Deliens, 1974), and (ii) heterogenite 2H, which is a hexagonal polytype defined by Deliens and Goethals (1973). Recent Raman microspectroscopy analyses coupled with electron backscattered diffraction (EBSD), however have shown that heterogenite is commonly poorly crystallized Burlet et al. (2011).

In the Katanga Copperbelt, heterogenite is derived from the oxidation of primary sulfide minerals hosted in stratiform deposits. Mio-Pliocene weathering strongly concentrated Co in the near-surface oxidized ore, within the so-called "cobalt-cap" (Decrée et al., 2010; Gauthier and Deliens, 1999). The genesis of heterogenite in the general Mio-Pliocene geodynamic framework in the Katanga has been recently reinvestigated by Decrée et al. (2010).

Here, further insights into the processes responsible for heterogenite formation are investigated through the study of rare earth elements (REE) distribution. This is a powerful tool in understanding the formation of oxi-hydroxides (Pourret and Davranche, 2013) since the fractionation of REE can be used as a tracer of these processes.

In this paper, the REE distribution is studied on mineral separates that remain variably admixed with the host rock. These samples are therefore representative of the bulk Co oxidized ore. They are investigated using X-Ray diffraction and scanning electron microscopy (SEM) with energy-dispersive spectroscopy (EDS) in order to determine their mineralogical

assemblage. Besides these bulk analyses, *in situ* (electron microprobe and LA-ICP-MS) analyses have been acquired, avoiding any contamination from the host rock. The REE signature of heterogenite is obtained using the LA-ICP-MS. The electron microprobe analyses are needed to determine how much the heterogenite is mixed with Mn oxi-hydroxides. This parameter is important since Mn oxi-hydroxides are known to strongly affect the REE behaviour. Eventually, modeling is used to predict how the REE speciation and how these elements should behave in a multi-ligand groundwater in the presence of Mn oxi-hydroxide.

All together, these data allow to investigate precisely the REE speciation in relation with the geochemistry (and mineralogy) of heterogenite (and Co oxidized ore) samples. Therefore, they can be used to clarify the processes leading to the formation of Co oxidized ore during the weathering in the Katanga Copperbelt.

At a larger scale, the study dedicated to the REE behavior in heterogenite could be applied to other Co-Ni-Mn oxide mineralizations that form laterite (on serpentinized ultramafic rocks), as those present in New Caledonia (Llorca and Monchoux 1991), Cuba (Moa Bay; Roqué-Rossell et al. 2010), Cameroon (Nkamouna; Dzemua et al. 2013), Colombia (Cerro Matoso; Gleeson et al., 2004), Australia (Greenvale; Zeissink, 1969) and USA (Oregon; Hotz, 1964).

2. Geological setting

The Cu-Co deposits of the Katanga Copperbelt are predominantly hosted in the lower part of the Neoproterozoic Katanga Supergroup (Roan Group, 880-730 Ma; Kampunzu et al., 2009) (**Figure 1**). The overlying deposits are part of the barren upper Roan (R-4, Mwashya Subgroup), Nguba (730-635 Ma) and Kundelungu (635-~573 Ma) Groups (ages after Kampunzu et al., 2009). The primary stratabound Cu-Co mineralization is typically hosted by metasedimentary rocks belonging to the lower part of the Roan Group (Faults and Roan

breccias on **Figure 1**). These host-rocks comprise dolomitic siltstones, stromatolitic dolostones, siltstones, dolomitic and carbonaceous shales, together with local sandstones and arkoses (Cailteux et al., 2005). The mineralization is also observed in brecciated and faulted lithotypes occurring mainly in the lower part of the Kundelungu Group (**Figure 1**). The primary stratiform Cu-Co sulfide mineralization is early syn-diagenetic (Dewaele et al., 2006; El Desouky et al., 2010; Muchez et al., 2008) and occurred around 820 Ma (Selley et al., 2005) and/or after ~750 Ma (Hitzman et al., 2005). Later mineralization events took place before or during the pan-African Lufilian folding (Cailteux et al., 2005; Decrée et al., 2011; Decrée et al., 2014; Dewaele et al., 2006; El Desouky et al., 2009; Haest and Muchez, 2011; Haest et al., 2007; Haest et al., 2009; Kampunzu et al., 2009). In these primary deposits, carrollite ($CuCo_2S_4$), siegenite ($(Ni,Co)_3S_4$) and linnaeite ($Co^{2+}Co^{3+}{}_2S_4$) are the most abundant primary cobalt ore minerals.

The post-orogenic history of the mineralization is poorly known. During this period, the Lufilian fold-and-thrust belt underwent various stages of weathering and erosional episodes. As a result, the sulfide ore deposits are now oxidized, usually down to a depth of ~100 m (Ngongo, 1975). Recent studies have shown that the Katanga Cu-Co oxidized ore is the result of a Pliocene weathering/oxidizing episode (SIMS U-Pb age of the heterogenite is dated at 3.4 ± 0.8 Ma; Decrée et al., 2010). This weathering process is economically significant because it strongly concentrated Co in the supergene ore when compared to the primary ore (64% Co for heterogenite *v*. 39% Co for carrollite). Heterogenite is thought to have formed in (sub)surface oxidizing conditions, whereas Cu migrates deeper downward and precipitates as malachite near the water table (De Putter et al., 2010; Decrée et al., 2010). Heterogenite caps can therefore be considered as a residual deposit, similar to iron-rich laterites.

3. Material and methods

The 24 heterogenite samples studied here originate from cobalt caps in 14 mines (see location on **Figure 1**). The samples were either collected in the field or recovered from the mineral collection in the Royal Museum for Central Africa, Tervuren, Belgium (**Table 1**). Mineral separates of these samples have been prepared. However, due to the intimate mixing of heterogenite with the host rock (especially when heterogenite impregnates earthy material), these samples are more representative of the bulk ore than pure heterogenite.

The texture of the samples was studied using scanning electron microscopy (SEM) on a Quanta 20 ESEM (FEI), with energy-dispersive spectroscopy (Apollo 10 Sillicon Drift EDS detector; EDAX) at the Royal Belgian Institute of Natural Sciences. The mineralogy of the rock samples was determined using a Bruker–Siemens X-ray micro-diffraction instrument equipped with a Cu Kα X-ray tube (operating at 40 kV and 30 mA), and a General Area Detector Diffraction System (GADDS) detector system at the ‘‘Laboratoire de Géochimie et Minéralogie appliquée” (Université Libre de Bruxelles), Belgium. Samples were scanned from 2-70°2θ and the software EVA 2, version 13 equipped with the JCPDS PDF-2 database (ICDD, 2003) was used for qualitative analysis of XRD patterns.

Quantitative micro-analyzes were acquired using a Cameca SX50 electron microprobe at the University of Mons operated at 15 kV / 20 nA with a defocused 20 µm diameter beam (Supplementary material, **Table 1**). The microprobe is equipped with four wavelength-dispersive (WDS) spectrometers and standard LIF, PET, TAP and PCs crystals.

Geochemical analyzes (major and trace elements, Supplementary material, **Tables 2 and 3**) were performed on representative powders (50 grams) of the heterogenite separates/Co oxidized ore at Actlabs, Ontario, Canada. To get the major elements and REE contents, the samples have been dissolved by lithium metaborate/tetraborate fusion, then digested in weak nitric acid solution before being analyzed by ICP-MS. Co and Cu contents have been obtained

after acid digestion by four different acids (hydrochloric, nitric, perchloric and hydrofluoric) and ICP-OES analyses.

Laser ablation ICP-MS measurements (Supplementary material, **Table 4**) were performed at the Geology and Mineralogy Department, Royal Museum for Central Africa, Belgium. A New-Wave UP-193 FX fast excimer (193 nm) laser coupled with a Thermo Scientific X-Series2 quadrupole ICP-MS was used. The laser was run at 50 Hz and a fluence of 10 J/cm^2 for a 100 µm spot size. He gas was flushed into the ablation cell at a flow rate of 0.65 L/min and was mixed afterwards in the cell with Ar carrier gas at a flow rate of 0.76 L/min. Co has been used as an internal standard for correcting instrumental drift and ablation rate. The NIST SRM 614, 612 and 610 were used as external standards and were measured frequently during the course of analyzes. The precision at 1 sigma level on the NIST SRM 612 is below 10% RSD.

The stability diagrams were modelled using the computer programs PHREEQC (Parkhurst and Appelo, 1999) and PhreePlot (Kinniburgh and Cooper, 2009). Both programs used the llnl.dat data base, which was modified to include well-accepted infinite-dilution (25 °C) stability constants for Co and Mn (Chivot et al., 2008; Collins and Kinsela, 2010; Hem et al., 1985).

The speciation calculations were performed using the computer program PHREEQC (Parkhurst and Appelo, 1999) using NAGRA/PSI data base (Hummel et al., 2002), which was modified to include well-accepted infinite-dilution (25 °C) stability constants for REE inorganic complexes (hydroxide, fluoride, chloride, sulfate and carbonate; Klungness and Byrne, 2000; Luo and Byrne, 2004; Migdisov et al., 2009; Schijf and Byrne, 2004) and surface complexation with hydrous manganese oxides (Pourret and Davranche, 2013).

4. Results

4.1. Typology, paragenesis and chemistry of the Katanga heterogenite

Macroscopically, the heterogenite specimens studied here occur as: (i) large (cm scale) reniform masses, (ii) massive impregnation of the silicified host-rock, in which quartz constitutes the dominant mineral phase, or (iii) earthy material finely admixed with the host-rock at an infra-µm scale, i.e. which is not visible using the SEM (see **Table 1** for further details). Under the microscope, heterogenite (3R polytype, see XRD patterns in **Figure 2**) is commonly present as small and finely laminated (µm to mm-thick laminae) nodular aggregates or botryoids (**Figure 3A-L**). These nodules include intercalations of heterogenite finely co-precipitated with Mn(-Fe) with oxides (mostly manganite and asbolane, as determined using XRD) and growths on a core made up of goethite or lepidocrocite (**Figure 2**). In the samples where heterogenite impregnates the host-rock or exhibits an earthy texture, quartz grains or phyllosilicate flakes are enclosed within the Co oxide (**Figures 3B,C,D,K**). Cuprite is present in association with heterogenite in several samples (**Figures 3C,D**).

From a geochemical point of view, heterogenite shows a wide range of Co concentration (16.9-86.4 wt. % Co_2O_3). The low Co content is generally related to the enrichment in other metals such as Cu (up to 24.5 wt. % CuO), Fe (up to 3.1 wt. % Fe_2O_3), Mn (up to 54.6 wt. % MnO_2), or Ni (up to 20.6 wt. % NiO). This is likely due to (1) the co-precipitation/intergrowth of heterogenite with other oxides, (2) metal substitution in the crystal lattice of heterogenite, and (3) the adsorption of these elements onto heterogenite. Low to moderate P enrichment (up to 1.9 wt. % P_2O_5) is observed in heterogenite. They are presumably related to the coprecipitation of heterogenite with secondary minerals resulting from the weathering of phosphates associated with Co-sulfides in the primary paragenesis. In addition, heterogenite may be enriched in U (from a few mg/kg to 3.2 wt.%) and Pb (see Decrée et al., 2014 for additional data about samples GE 10788 and GE 10816).

Among the minerals that form in Co-Ni-Mn laterite-like deposits, heterogenite shows the highest Co contents when compared to (1) absolane-lithiophorite minerals from Nkamouna (2.3-17.0 wt.% CoO; Dzemua et al., 2013), New Caledonia (0.9-12.6 wt.% CoO; Llorca and Monchoux 1991) and Moa Bay (1.2-7.8 wt.% CoO; Roqué-Rossell et al., 2010) and (2) cryptomelane, pyrolusite and other Mn oxides from Nkamouna (with 0.7-16.9 wt.% CoO; Dzemua et al., 2013). Additionally, most of the Katanga heterogenites possess the highest ratios of Co against Mn, Al, Ni, and plot very close to the Co pole in Co-Al-Ni and Co-Ni-Mn ternary diagrams (**Figure 4**). Heterogenite in Mn-rich layers are rather close in composition to the pyrolusite and "lithiophorite-asbolane intermediate" from the Nkamouna area.

4.2. Heterogenite separates – cobalt oxidized ore (whole rock signatures)

Selected major and trace elements of the studied samples are presented as **Supplementary material**. Heterogenite is characterized by high but variable Co contents, ranging from 18.44 to 68.79 wt.% CoO. It also contains variable contents of Cu (0.48-16.8 wt.% CuO), Mn (0.01-4.81 wt.% MnO) and Fe (0.12-16.26 wt.% Fe_2O_3(t)). These elements are part of the heterogenite structure or represent a fine admixture of cuprite or Fe/Mn-oxides (see **Figure 1**). The high SiO_2 contents observed in most samples are due remnants of host-rock minerals in the Co oxidized ore (e.g., in **Figure 3B**). The high P_2O_5 contents in samples RGM 4418 and RGM 13025 are attributed to the presence of phosphates. Three analyzed samples (i.e., RGM 3335, RGM 14091 and RGM 10794), which are admixed with Mn-oxides or the host-rocks, show particularly low Co contents (i.e., 11.25, 4.79 and 2.64wt.% CoO, respectively).

Co enrichment in Katanga heterogenite ore is particularly well highlighted in the Co-Al-Ni and Co-Ni-Mn diagrams (**Figure 4**), when compared to Co-bearing nickeliferous laterites from Cerro Matoso (Colombia), Greenvale (Australia) and Oregon (USA). In these

lateritic ores, the CoO content is below 0.6 wt.% (Gleeson et al., 2004; Hotz, 1964; Zeissink, 1969).

4.3. Rare earth element signatures

4.3.1. Heterogenite separates – cobalt oxidized ore (whole rock signatures)

The Upper Continental Crust (UCC)-normalized rare earth element (REE) analyzes of the heterogenite samples show three distinct types of patterns. Type 1 patterns show low total REE abundance ($14<\Sigma REE<122$ mg/kg, with a mean value of 70 mg/kg) and displays a distinctive bell-shaped pattern (**Figure 5A**), with $\log (La/Sm)_{UCC}<1$ and $\log (Gd/Yb)_{UCC}>1$ (quadrant 1 in **Figure 6A**). These samples commonly show a negative cerium anomaly (Ce/Ce* from 0.1 to 1), with no significant europium anomaly (Eu/Eu* from 0.7 to 1.6 with an exception at 3 for sample RGM 2839). Type 2 patterns show REE light REE (LREE) enrichment (ΣREE= 524 and 1436 mg/kg; La_{ucc}/Yb_{ucc}= 30 and 73; **Figure 5B**), with $\log (La/Sm)_{UCC}>0$ and $\log (Gd/Yb)_{UCC} >0$ (quadrant 2 in **Figure 6A**). There is no significant Ce anomaly (Ce/Ce* = 0.6 and 1) and the Eu anomaly is slightly positive or negative (Eu/Eu*= 0.4 and 1.2). Type 3 patterns are rather flat from La to Eu but with a slight Heavy REE (HREE) fractionation (**Figure 5C**). It is intermediately enriched in REE (ΣREE= 133 and 142 mg/kg) compared to the other types, with a positive Eu anomaly (Eu/Eu* = 1.6 and 1.8) and no marked Ce anomaly (Ce/Ce*=~0.8). In the $\log (Gd/Yb)_{UCC}$ vs. $\log (La/Sm)_{UCC}$ diagram (**Figure 6A**), these heterogenites plot at the boundary between quadrant 1 and 2.

4.3.2. LA-ICP-MS signatures

Due to the intimate mixing of heterogenite with host rock minerals in the impregnation and earthy facies, *in situ* (LA ICP-MS) analyzes have been performed to obtain the REE signature of these minerals. Compared to the corresponding whole rock patterns, the Type 1 LA-ICP-

MS REE patterns display a similar MREE enrichment (**Figure 5D**), with quite comparable REE contents (4<ΣREE<111 mg/kg, with an exception at 321 mg/kg for sample RGM 13017), and negative or slightly positive Ce and Eu anomalies (0.01< Ce/Ce*<1.4 and 0.3<Eu/Eu*<1.3, with an exception at 2.5 for sample RGM 12979). On the other hand, LA-ICP-MS REE patterns obtained on Type 2 heterogenites differ from the whole rock REE patterns (**Figure 5E**): they are slightly HREE or MREE-enriched, with negative Ce and Eu anomalies (0.02<Ce/Ce*<0.8 and 0.4<Eu/Eu*<1.1). In addition, the total REE contents are very low (from 2 to 7 mg/kg). LA-ICP-MS REE patterns for the third type of heterogenites resemble those obtained from whole rock analyzes, with negative Ce anomaly (Ce/Ce* = 0.5 and 0.7) and positive Eu anomaly (Eu/Eu* = 1.2 and 1.3). They are however less enriched in REE (ΣREE = 30 and 49 mg/kg), especially in LREE, highlighting a slight MREE enrichment in the patterns. In the log $(Gd/Yb)_{UCC}$ vs. log $(La/Sm)_{UCC}$ diagram (**Figure 6C**), most of the heterogenites plot in the quadrant I (log $(La/Sm)_{UCC}$<0 and log $(Gd/Yb)_{UCC}$>0).

5. Discussion

Based on whole rock analyzes, it appears that heterogenite commonly exhibits three types of REE patterns. Type 1 is enriched in middle REE, with a negative Ce anomaly and a relatively low REE content. Types 2 and 3 are variably enriched in LREE, without a Ce anomaly and with higher REE content. However, *in situ* LA-ICP-MS analyses reveal that the LREE enrichment of the Types 2 and 3 patterns is not related to heterogenite itself. This enrichment is likely due to a mineral phase that is associated with heterogenite in the bulk Co oxidized ore.

The aim of this discussion is (1) to investigate the fractionation of the REE in a supergene environment where both heterogenite and Mn-oxides form, (2) to study and model

the speciation of the REE in groundwaters, and (3) to provide an improved conceptual model of heterogenite formation**.**

5.1. Supergene formation of heterogenite and REE competition with coeval Mn-oxides

Heterogenite is a supergene mineral that precipitates from aqueous solution saturated in Co (Chivot et al., 2008; Deliens, 1974; Myers and Penn, 2011). In the Katanga Copperbelt, heterogenite is deposited by near-surface fluids whereas Cu remains in the solution and percolates downwards (Decrée et al., 2010). These processes are overall similar to those leading to the formation of other supergene deposits that develop on various metasedimentary rocks in Katanga, including the Kisenge Mn-oxide rich caps and the widely exposed Fe-laterites (Decrée et al., 2010).

In this environment, heterogenite behaves similar to manganese oxide. CoOOH and MnOOH have the same bond length 1.92 Å and similar Co-(Co, Mn) and Mn-Mn distances 2.79 vs 2.81 (Brown and Calas, 2012). Cobalt is strongly enriched in supergene deposits because it is oxidized from Co^{2+} to the less soluble Co^{3+} in supergene conditions, possibly through a disproportionation process as described by Hem (1978). Mn-oxide colloids scavenge trace metals via adsorption – and/or co-precipitation - where hydrated cations (e.g., REE) are attracted to the negatively charged surface of manganese oxides (e.g., Pourret and Davranche, 2013). At high Co activity, heterogenite (**Figure 7A**) precipitates at near-neutral pH conditions as well as manganese oxide (i.e., pyrolusite, **Figure 7B**).

In **Figure 8**, one can see that the increase of the Ce/Ce*,La_{UCC}/Yb_{UCC}, La_{UCC}/Sm_{UCC} and Gd_{UCC}/Yb_{UCC} ratios is correlated with an increase of the MnO content. As a whole, the total REE content is also correlated to the increase in MnO. More precisely, two different trends are observed: the first trend (green arrow in **Figure 8**) shows a rapid increase of the above-mentioned ratios and REE content for a slight increase of MnO content. Whereas the

second one (orange arrow in **Figure 8**) is characterized by a moderate increase of the above-mentioned ratios and content for higher MnO contents. The presence of two different trends could be related to the presence of various Mn-oxides in association with heterogenite. Manganite, asbolane and lithiophorite are actually commonly encountered in the Co oxidized ore, even within a single specimen. Heterogenite is also commonly amorphous or poorly-crystalline, with size below micrometer (Burlet et al., 2011). In addition, Mn- and Co-oxides may have highly variable crystallinity at microscopic scale and this is likely to influence important characteristics such as specific surface and adsorption kinetic, even within a single sample.

Despite their mineralogical similarities, Mn-oxides associated with heterogenite should present less fractionated REE patterns (no or less MREE enrichment), with positive Ce anomalies and a higher REE enrichment compared to heterogenite. Such patterns are commonly found for Mn-oxides in similar environments, for example in Fe-Mn laterites present in the Katanga Copperbelt (**Figure 10**). Consequently, the weathering process has resulted in the mobilization and redistribution of the REE affected by the nature of secondary mineral formation (e.g., Mn oxi-hydroxides).

5.2. REE speciation in alkaline groundwater

5.2.1. Alkaline nature of the groundwater during heterogenite formation

The presence of aqueous ligands, notably carbonate or hydroxide in water strongly affects REE solubility (Woods, 1990; Leybourne and Johannesson, 2008). Release of REE during weathering is strongly controlled by dissolution rates of parent rock minerals. In the Katanga Copperbelt, the Mio-Pliocene weathering event led to the dissolution of the Mines Subgroup dolomites and dolomitic shales, and the formation of karst (Buffard, 1984; De Putter et al., 2010) and heterogenite (Decrée et al., 2010). This dissolution should result in a neutral to

alkaline fluid with the carbonate ion dominating in the solution. Locally, sulfate and phosphate ions could play a more important role due to dissolution and alteration of sulfides and P-bearing minerals such as monazite, apatite, dahlite [$Ca_5(PO_4,CO_3)_3F$] (Kampunzu et al., 2005). Stability and composition of accessory minerals play a dominant role in the availability and mobility of trace elements. Indeed the formation of secondary REE-minerals present as secondary mineral phases in the Katanga Copperbelt (e.g., florencite-(La), françoisite-(Nd), gysinite-(Nd), kamotoïte-(Y), lepersonnite-(Gd), schuilingite-(Nd), shabaite-(Nd), bijvoetite-(Y); Daltry, 1992) can give us some clues for deciphering the probable ligands present in the supergene ore-forming fluid (i.e., carbonates).

A simple weathering scheme, primarily based on a change in fluid chemistry, can explain such observations. Acidic rain water – equilibrated with atmospheric CO_2 – has a pH of ~5.7. In contact with the uppermost part of the soil, the pH of this fluid can decrease up to 4-5, due to the decay of organic material (Nesbitt, 1979; Pourret et al., 2016). These acidic and oxidized fluids will percolate through the host rock (mineralized siltstones, shales and dolostones). As a result, (1) the mineralized host rocks are weathered, (2) the soluble major, minor and REE are removed, and (3) the fluids are progressively neutralized by the carbonates. Subsequently, in the upper part of the weathering profile (where the Type 1 – MREE-rich – heterogenite forms), the REE are mainly adsorbed onto the surface of the neoformed secondary minerals (i.e., manganese oxides and heterogenites; **Figure 7**). At these circumneutral pH, the speciation of the REE is mainly driven by the carbonate ions, the HREE being mobilized to a greater extent than the LREE (e.g. Johannesson et al., 1996). These solutions – which are still enriched in metals and REE - then migrate downwards, with a concomitant increase in the pH. As the fluid becomes more alkaline, the REE are precipitated as carbonates (LREE-rich mineral co-precipitated with heterogenite as evoked in **Figures 5 E,F**) , incorporated into/precipitated as secondary minerals, or adsorbed onto

manganese oxides and heterogenites.

5.2.2. Calculation of REE speciation in the multi-ligand groundwater

In order to calculate REE speciation in groundwater while no groundwater analyses were performed on the study area (e.g. Atibu et al., 2013), the multi-ligand groundwater from Wood (1990) was used. The speciation of La^{3+}, Eu^{3+}, Lu^{3+} in the multi-ligand groundwater at 25°C (given in Table VIII in (Wood, 1990)) taking into account two concentrations of manganese (allowing REE adsorption onto hydrous manganese oxide) was calculated by simultaneously solving the relevant mass-action and mass-balance equations at each pH using PHREEQC and PhreePlot (see section 3 for details). The concentrations of manganese were selected to represent concentrations in superficial waters (Pettersson and Ingri, 2001; Sracek et al., 2012). The ligands (i.e., chlorides, sulfates, carbonates) present in the multi-ligand groundwater from Wood (1990) are similar to those considered by Muchez and Corbella (2012) at 150°C.

The results of these calculations are depicted in **Figure 9**. In the model groundwater with higher Mn concentrations (i.e., 10-4 mol/L), it is evident from figures 9A-C that La, Eu and Lu: (1) exist predominately as the simple ion REE^{3+} and the sulfate complex $REESO_4^+$ at pH=4-6.5, (2) are adsorbed on manganese oxide at pH = 6.5-7.5, (3) occur as the carbonate complex $REECO_3^+$ at pH=7.5-9.5, and (4) are present as the hydroxide complex $REEOH^{2+}$ at pH >9.5. In the modeling conditions considered for figures 9A-C, only the carbonate and sulfate complexes are stable enough to significantly affect REE transport (e.g., Johannesson, 2005). More precisely, at neutral pH (expected values of samples), fractionation occurs in between REE. At pH 6, La and Eu are only weakly adsorbed onto Mn oxide (<10%), whereas Lu is strongly adsorbed to Mn oxide (>30%). Such modeling results highlight the scenario (and resulting REE fractionation) that could occur in the upper zone of the weathering profile

where Type 1 heterogenite (characterized by MREE enrichment**; Figures 5 A,D**) forms. Figures 9D-F further illustrate the effect on speciation by changing the various ligand concentrations used in the model. This second modeling scenario highlight the conditions favorable for precipitation of Types 2 and 3 heterogenite and controlled by carbonates (with the probable coprecipitation of heterogenite with a LREE carbonate; **Figures 5 A,B,E,F**). Actually, if the total manganese concentration is decreased by an order of magnitude then the carbonate complexes become important from pH 6.5 to 9.5 (**Figures 9D-F**). The carbonate complexes of the REE are thus the most important inorganic species competing with Mn oxi-hydroxide and responsible for the transport of REE in near neutral to slightly alkaline groundwaters. The dominant carbonate complex for LREE is $LREECO_3^+$, whereas for HREE a complex $HREECO_3^{2-}$ dominates in solution (Luo and Byrne, 2004). Among inorganic complexes, carbonate complexes are more frequent in the pH range 7 to 9; above pH 9 hydroxyl complexes prevail, and below pH 7 REE^{3+} ions dominate, whereas the role of sulfate is subordinated (Schijf and Byrne, 2004). An increase in pH decreases the role of REE^{3+} ions, especially for HREE. The presence of Mn oxi-hydroxide substantially changes existing REE complexes. Thus, Mn oxi-hydroxides prevail within the pH interval 6.5 to 9 (Pourret and Davranche, 2013). At lower pH, REE^{3+} ions are relatively more abundant and sulfate complexes such as $REESO_4^+$ may appear, whereas an increase in pH leads to an increase in the role of carbonate (Wood, 1990). In this context, the impact of organic matter on REE speciation was not considered even though Tang and Johannesson (2003) and Pourret et al. (2007) demonstrated their major influence. It should also be noted that all of the estimations above are based on certain assumptions, such as equal activity of all species, comparably low REE concentration and absence of competing cations in the solution.

5.3. Improved conceptual model of heterogenite formation

At high Co activity, heterogenite precipitates at near-neutral pH conditions as well as manganese oxide (i.e., manganite). REE are mainly fractionated between these two solid phases (**Figure 10**). As cobalt activity decreases, the heterogenite stability field shifts towards an alkaline pH. In these conditions, REE speciation is mainly driven by carbonate complexation and/or precipitation. Since the heterogenite patterns are enriched in LREE (**Figures 5 B,C,E,F**), one can consider that a LREE-rich carbonate co-precipitates with and/or is adsorbed onto heterogenite. This scheme is likely since (i) there is no correlation between REE and MnO or P_2O_5 contents in the studied whole rock and (ii) REE-carbonates (as gysinite-(Nd) [$Pb(Nd,La)(CO_3)_2(OH).H_2O$]) are found in the oxidized part of numerous deposits of the Katanga Copperbelt (Daltry, 1992). In any case, the association of heterogenite with this mineral gives the LREE-rich Type 2 and Type 3 patterns illustrated in **Figures 5B and 5C**.

Both REE signatures (MREE-enriched Type 1 on the one hand and LREE-enriched Types 2 and 3 on the other hand) are consistent with the formation of heterogenite in a two-step *per descensum* model, in which this mineral (i) forms as residual deposits - similar to laterite - in association with Mn-oxide, in the immediate near-surface environment, with an obvious REE fractionation between these two mineral phases, and (ii) is deposited from a carbonate-bearing fluid due to country rock dissolution in the deeper parts of the oxidation profile, in association with REE-rich carbonates (**Figure 10**).

The weathering of primary sulfide minerals (carrollite from the Kamoto mine, sample RGM 13024, and siegenite from the Shinkolobwe mine, sample GE 3101, **Figure 5A**) constitutes an important mobile REE reservoir. As demonstrated in **Figure 5A**, heterogenite actually displays REE patterns that are quite close to the parental Co-sulfides, being more enriched that the latter but with preservation and even enhancement of the MREE-enrichment. The processes leading to the incorporation of REE into heterogenite could certainly be

compared to those invoked to explain the preservation of the isotopic U-Pb system within heterogenite (Decrée et al., 2014), namely the trapping of relict nanoparticles and/or the sorption of these elements. By passing through Mn-rich horizons the fluids become enriched in manganese and thereby promote REE release from their carbonate support favouring Mn oxides sorption (Pourret et al., 2014). Finally, the observed cerium anomalies are interpreted to be the result of oxidizing conditions affecting the valence state of Ce, especially oxidation scavenging together with Mn oxi-hydroxides (Pourret et al., 2014).

6. Concluding remarks

Heterogenite (CoOOH) was deposited by near-surface fluids during the weathering of the sulfide-bearing Mine Series, in the Katanga Copperbelt. A detailed study of this supergene deposit based on bulk and LA-ICP-MS analyzes gives new keys to understand the processes leading to heterogenite formation. Heterogenite commonly exhibits the following REE characteristics: a MREE-enriched pattern, negative Ce anomaly and overall low concentration in REE. When heterogenite is finely admixed with Mn-oxides, the resulting REE patterns are flatter, the negative Ce anomaly is smaller (or may even be slightly positive) and the total concentration in REE is higher. This suggests that fractionation of REE occurs between Co- and Mn-oxide minerals in the upper part of the weathering profile. In the deeper part of the profile, Co activity decreases and the downward migration of the fluids induces dolostone dissolution. As a consequence, heterogenite precipitates from alkaline groundwater in association with a LREE-rich mineral, which notably controls the REE speciation.

Acknowledgments

This study is a contribution to the GECO project, funded by the Belgian Federal Public Service for Foreign Affairs. The author would like to warmly thank the MRAC for providing

the study samples. Luc André and Laurence Monin are also thanked for their role in providing LA-ICP-MS analyzes. Editors and an anonymous reviewer are sincerely thanked for the editorial handling of the manuscript and their help to improve the quality of this work. Thomas Goovaerts (RBINS) is thanked for the English reviewing of the manuscript.

References

Atibu, E. K., Devarajan, N., Thevenon, F., Mwanamoki, P. M., Tshibanda, J. B., Mpiana, P. T., Prabakar, K., Mubedi, J. I., Wildi, W., Poté, J., 2013. Concentration of metals in surface water and sediment of Luilu and Musonoie Rivers, Kolwezi-Katanga, Democratic Republic of Congo. Applied Geochemistry 39, 26-32.

Brown, G.E., Calas, G., 2012. Mineral-Aqueous Solution Interfaces and Their Impact on the Environment. Geochemical Perspective 1 (4-5), 483-742.

Burlet, C., Vanbrabant, Y., Goethals, H., Thys, T., Dupin, L., 2011. Raman spectroscopy as a tool to characterize heterogenite (CoO·OH) (Katanga Province, Democratic Republic of Congo). Spectrochimica Acta - Part A: Molecular and Biomolecular Spectroscopy 80 (1), 138-147.

Byrne, R.H., Li, B., 1995. Comparative complexation behavior of the rare earths. GeochimIca et Cosmochimica Acta 59, 4575-4589.

Cailteux, J.L.H., Kampunzu, A.B., Lerouge, C., Kaputo, A.K., Milesi, J.P., 2005. Genesis of sediment-hosted stratiform copper–cobalt deposits, central African Copperbelt. Journal of African Earth Sciences 42 (1–5), 134-158.

Chivot, J., Mendoza, L., Mansour, C., Pauporté, T., Cassir, M., 2008. New insight in the behaviour of Co-H2O system at 25-150 °C, based on revised Pourbaix diagrams. Corrosion Science 50 (1), 62-69.

Collins, R.N., Kinsela, A.S., 2010. The aqueous phase speciation and chemistry of cobalt in terrestrial environments. Chemosphere 79 (8), 763-771.

Daltry, V.D.C., 1992. The type mineralogy of Africa: Zaire. Annales de la Société Géologique de Belgique 115, 33-62.

De Putter, T., Mees, F., Decrée, S., Dewaele, S., 2010. Malachite, an indicator of major Pliocene Cu remobilization in a karstic environment (Katanga, Democratic Republic of Congo). Ore Geology Reviews 38 (1–2), 90-100.

De Putter, T., Decrée, S., Banza Lubaba Nkulu, C., Nemery, B., 2011. Mining the Katanga (DRC) Copperbelt: geological aspects and impacts on public health and the environment – towards a holistic approach. IGCP/SIDA Project 594, Inaugural Workshop, Kitwe, Zambia, book of abstracts, 14-17. Available online at: http://www.geology.cz/igcp594/kitwe/PROCEEDINGS-OF-THE%20WORKSHOP.pdf

Decrée, S., Deloule, E., Ruffet, G., Dewaele, S., Mees, F., Marignac, C., Yans, J., De Putter, T., 2010. Geodynamic and climate controls in the formation of Mio-Pliocene world class oxidized cobalt and manganes ores in the Katanga province, DR Congo. Mineralium Deposita 45, 621-629.

Decrée, S., Deloule, É., De Putter, T., Dewaele, S., Mees, F., Yans, J., Marignac, C., 2011. SIMS U–Pb dating of uranium mineralization in the Katanga Copperbelt: Constraints for the geodynamic context. Ore Geology Reviews 40 (1), 81-89.

Decrée, S., Deloule, E., De Putter, T., Dewaele, S., Mees, F., Baele, J.M., Marignac, C., 2014. Dating of U-rich heterogenite from the Katanga Copperbelt: new insights into U deposit genesis and U cycling. Precambrian Research 241, 17-28.

Deliens, M., 1974. Les Oxydes Hydrates de Cobalt du Shaba Méridional. Annales du Musée Royal de l'Afrique Centrale, Sciences Géologiques 76, 80 p.

Deliens, M., Goethals, H., 1973. Polytypism of heterogenite. Mineralogical Magazine 39, 152-157.

Dewaele, S., Muchez, P., Vets, J., Fernandez-Alonzo, M., Tack, L., 2006. Multiphase origin of the Cu-Co ore deposits in the western part of the Lufilian fold-and-thrust belt, Katanga (Democratic Republic of Congo). Journal of African Earth Sciences 46 (5), 455-469.

Dzemua GL, Gleeson SA, Schofield PF (2013) Mineralogical characterization of the Nkamouna Co–Mn laterite ore, southeast Cameroon. Miner Deposita 48:155–171.El Desouky, H.A., Muchez, P., Cailteux, J., 2009. Two Cu-Co sulfide phases and contrasting fluid systems in the Katanga Copperbelt, Democratic Republic of Congo. Ore Geology Reviews 36 (4), 315-332.

El Desouky, H.A., Muchez, P., Boyce, A.J., Schneider, J., Cailteux, J.L.H., Dewaele, S., von Quadt, A., 2010. Genesis of sediment-hosted stratiform copper-cobalt mineralization at Luiswishi and Kamoto, Katanga Copperbelt (Democratic Republic of Congo). Mineralium Deposita 45 (8), 735-763.

François, A., 1974. Stratigraphie , tectonique et minéralisations dans l'Arc cuprifère du Shaba (Rép.du Zaïre), in: Bartholomé, P. (Ed.), Gisements stratiformes et provinces cuprifères. Centenaire de la Société Géologique de Belgique, Liège, pp. 79–101.

Gauthier, G., Deliens, M., 1999. Cobalt minerals of the Katanga Crescent, Congo. Mineralogical Records 30 (4), 255-273.

Gleeson, S.A., Herrington, R.J., Durango, J., Velasquez, C.A., Koll, G., 2004. The Mineralogy and Geochemistry of the Cerro Matoso S.A. Ni Laterite Deposit, Montelíbano, Colombia. Economic Geolology 99, 1197-1213.

Haest, M., Muchez, P., 2011. Stratiform and Vein-Type Deposits in The Pan-African Orogen in Central and Southern Africa: Evidence for Multiphase Mineralisation. Geologica Belgica 14 (1-2), 23-44.

Haest, M., Muchez, P., Dewaele, S., Boyce, A.J., von Quadt, A., Schneider, J., 2009. Petrographic, fluid inclusion and isotopic study of the Dikulushi Cu-Ag deposit, Katanga (D.R.C.): Implications for exploration. Mineralium Deposita 44 (5), 505-522.

Haest, M., Muchez, P., Dewaele, S., Franey, N., Tyler, R., 2007. Structural control on the Dikulushi Cu-Ag deposit, Katanga, Democratic republic of Congo. Economic Geolology 102 (7), 1321-1333.

Hem, J.D., 1978. Redox processes at surfaces of manganese oxide and their effects on aqueous metal ions. Chemical Geology 21 (3–4), 199-218.

Hem, J.D., Roberson, C.E., Lind, C.J., 1985. Thermodynamic stability of CoOOH and its coprecipitation with manganese. Geochimica et Cosmochimica Acta 49 (3), 801-810.

Hey, M.H., 1962. Cobaltic hydroxyde in nature. Mineralogical Magazine 33, 253-259.

Hitzman, M., Kirkham, R., Broughton, D., Thorson, J., Selley, D., 2005. The sediment-hosted stratiform copper ore system, Economic Geology: one hundredth anniversary volume, 1905-2005. Society of Economic Geologists, Littleton, CO, USA, pp. 609-642.

Hotz, P.E., 1964. Nickeliferous laterites in Southwestern Oregon and Northwestern California. Economic Geology 59, 355-396.

Hummel, W., Berner, U., Curti, E., Pearson, F.J., Thoenen, T., 2002. Nagra / PSI Chemical Thermodynamic Data Base 01/01. Universal Publishers, Parkland, Florida.

ICDD, 2003. JCPDS PDF-2 database. ICDD, Newton Square, PA, U.S.A.

Johannesson, K.H., 2005. Rare Earth Elements in Groundwater Flow Systems. Springer, Dordrecht.

Johannesson, K.H., Stetzenbach, K.J., Hodge, V.F., Lyons, W.B., 1996. Rare earth element complexation behavior in circumneutral pH groundwaters: Assessing the role of carbonate and phosphate ions. Earth Planetary Science Letters 139, 305-319

Johannesson, K.H., Hendry, M.J., 2000. Rare earth element geochemistry of groundwaters from a thick till and clay-rich aquitard sequence, Saskatchewan, Canada. Geochimica et Cosmochimica Acta 64, 1493-1509.

Kampunzu, A.B., Cailteux, J.L.H., Moine, B., Loris, H.N.B.T., 2005. Geochemical characterisation, provenance, source and depositional environment of 'Roches Argilo-Talqueuses' (RAT) and Mines Subgroups sedimentary rocks in the Neoproterozoic Katangan Belt (Congo): Lithostratigraphic implications. Journal of African Earth Sciences 42 (1–5), 119-133.

Kampunzu, A.B., Cailteux, J.L.H., Kamona, A.F., Intiomale, M.M., Melcher, F., 2009. Sediment-hosted Zn-Pb-Cu deposits in the Central African Copperbelt. Ore Geology Reviews 35 (3-4), 263-297.

Kinniburgh, D.G., Cooper, D.M., 2009. PhreePlot: Creating graphical output with PHREEQC. Available at: http://www.phreeplot.org, p. 498.

Klungness, G.D., Byrne, R.H., 2000. Comparative hydrolysis behavior of the rare earths and yttrium: the influence of temperature and ionic strength. Polyhedron 19, 99-107.

Leybourne, M.I, Johannesson, K.H., 2008. Rare earth elements (REE) and yttrium in stream waters, stream sediments, and Fe-Mn oxyhydroxides: fractionation, speciation, and controls over REE + Y patterns in the surface environment. Geochimica et Cosmochimica Acta 72, 5962-5983.

Llorca S., Monchoux, P (1991) Supergene cobalt minerals from New-Caledonia. Canadian Mineralogist 29, 149-161

Luo, Y.-R., Byrne, R.H., 2004. Carbonate complexation of yttrium and the rare earth elements in natural rivers. Geochimica et Cosmochimica Acta 68, 691-699.

McLennan, S.M., 2001. Relationships between the trace element composition of sedimentary rocks and upper continental crust. Geochemistry Geophysics Geosystems, 2 (4).

Migdisov, A.A., Williams-Jones, A.E., Wagner, T., 2009. An experimental study of the solubility and speciation of the Rare Earth Elements (III) in fluoride- and chloride-bearing aqueous solutions at temperatures up to 300 °C. Geochimica et Cosmochimica Acta 73, 7087-7109.

Muchez, P., Corbella, M., 2012. Factors controlling the precipitation of copper and cobalt minerals in sediment-hosted ore deposits: Advances and restrictions. Journal of Geochemical Exploration 118, 38-46.

Muchez, P., Vanderhaeghen, P., Desouky, H., Schneider, J., Boyce, A., Dewaele, S., Cailteux, J., 2008. Anhydrite pseudomorphs and the origin of stratiform Cu - Co ores in the Katangan Copperbelt (Democratic Republic of Congo). Mineralium Deposita 43 (5), 575-589.

Myers, J.C., Penn, R.L., 2011. Controlling heterogenite particle morphology and microstructure by varying synthetic conditions. Material Research Bulletin 46, 649-657.

Nesbitt, H.W., 1979. Mobility and fractionation of rare earth elements during weathering of a granodiorite. Nature 279, 206-210.

Ngongo, K., 1975. Similarity Between the Uraniferous Deposits (Shinkolobwe Type) and the Cupriferous Deposits (Kamoto Type) at Shaba, Zaire. Annales de la Société Géologique de Belgique 98 (2), 449-462.

Parkhurst, D.L., Appelo, C.A.J., 1999. User's guide to PHREEQC (Version 2) - A computer program for speciation, batch-reaction, one-dimensional transport, and inverse

geochemical calculations. 99-4259, U.S. Geological Survey Water-Resources Investigations Report.

Pettersson, U.T., Ingri, J., 2001. The geochemistry of Co and Cu in the Kafue River as it drains the Copperbelt mining area, Zambia. Chemical Geology 177, 399-414.

Pourret, O., Davranche, M., Gruau, G., Dia, A., 2007. Rare Earth Elements complexation with humic acid. Chemical Geology 243, 128-141.

Pourret, O., Davranche, M., 2013. Rare earth element sorption onto hydrous manganese oxide A modeling study. Journal of Colloid Interface Sciences 395, 18-23.

Pourret, O., Lange, B., Jitaru, P., Mahy, G., Faucon, M.-P., 2014. Transfer of rare earth elements from natural metalliferous (copper and cobalt rich) soils into plant shoot biomass of metallophytes from Katanga (Democratic Republic of Congo). Geophysical Research Abstracts 16, EGU2014-6272.

Pourret, O., Lange, B., Bonhoure, J., Colinet, G., Decrée, S., Mahy, G., Séleck, M., Shutcha, M., Faucon, M.P., 2016 Assessment of soil metal distribution and environmental impact of mining in Katanga (Democratic Republic of Congo). Accepted to Applied Geochemistry.

Roqué-Rosell J, Mosselmans JFW, Proenza JA, Labrador M, Galí S, Atkinson KD, Quinn PD (2010) Sorption of Ni by "lithiophorite–asbolane" intermediates in Moa Bay lateritic deposits, eastern Cuba. Chemical Geology 275, 9-18

Schijf, J., Byrne, R.H., 2004. Determination of $SO_4\beta_1$ for yttrium and the rare earth elements at I = 0.66 m and t = 25 °C-Implications for YREE solution speciation in sulfate-rich waters. Geochimica et Cosmochimica Acta 68, 2825-2837.

Selley, D., Broughton, D., Scott, R., Hitzman, M., Bull, S.W., Large, R.R., McGoldrick, P., Croaker, M., Pollington, N., Barra, F., 2005. A new look at the geology of the

Zambian Copperbelt, Economic Geology: one hundredth anniversary volume, 1905-2005. Society of Economic Geologists, Littleton, CO, USA, pp. 965-1000.

Sracek, O., Kříbek, B., Mihaljevič, M., Majer, V., Veselovský, F., Vencelides, Z. Nyambe, I., 2012. Mining-related contamination of surface water and sediments of the Kafue River drainage system in the Copperbelt district, Zambia: An example of a high neutralization capacity system. Journal of Geochemical Exploration 112, 174-188.

Tang, J., Johannesson, K.H., 2003. Speciation of rare earth elements in natural terrestrial waters: Assessing the role of dissolved organic matter from the modeling approach. Geochimica et Cosmochimica Acta 67, 2321-2339.

USGS, 2013. Mineral Commodity Summaries 2014.

Wood, S.A., 1990. The aqueous geochemistry of the rare-earth elements and yttrium. 1. Review of the available low-temperature data for inorganic complexes and inorganic REE speciation in natural waters. Chemical Geology 82, 159-186.

Zeissink, H.E., 1969. The Mineralogy and Geochemistry of a Nickeliferous Laterite Profile (Greenvale, Queensland, Australia). Mineralium Deposita 4, 132-152.

Figure and Table Captions

Figure 1 Geological sketch map of the Copperbelt (modified from Cailteux et al., 2005; François, 1974). R-4 corresponds to the Mwashya Subgroup.

Figure 2 XRD patterns (Cu Ka) of representative heterogenites from the Katanga Copperbelt compared to the reference patterns (vertical lines) from the ‘‘International Centre for Diffraction Data” database (abbreviations used as follows: Ht for heterogenite, 3R for the 3R polytype, Qz for quartz, Gt for goethite, Lc for lepidocrocite, Mn for manganite, Asb for asbolan). A. Sample DOL1 from Luiswishi; B. Sample RGM 10801 from Kalabi; C. Sample RGM 10805 from Musonoi

Figure 3 SEM backscattered electron images illustrating heterogenite facies in the studied samples and the LA-ICP-MS analysed zones (numbers from 1 to 30). The sample name is indicated on each picture (refer to **Table 1** for sample origin). The abbreviations are as followed: Cu for cuprite, FeOX for Fe-oxides, Qz for quartz. A. Botryoidal heterogenite (brigh laminae) in alternation with Mn-rich oxide laminae (grey area) an in association with Fe oxide. B. Heterogenite concretion comprising quartz grains. The dark grey laminae correspond to Mn-rich layers. C. Mineral assemblage made up of heterogenite, quartz and cuprite in an earthy facies. D. Heterogenite concretion comprising quartz grains and is association with late cuprite concretion. The dark grey laminae correspond to Mn-rich layers. E. H. and I. Botryoidal heterogenite. F. and J. Botryoidal heterogenite. The dark grey laminae correspond to Mn-rich layers/zones. G. Heterogenite concretion associated with Fe oxide. K. Heterogenite concretion comprising quartz grains and phyllosilicate laths from the host-rock. L. Heterogenite concretion. The brighter layers correspond to laminae enriched in Pb and U. The dark zone results from the LA ablation.

Figure 4 Ternary diagrams showing the variations in terms of (A) Co-Al-Ni, (B) Co-Ni-Mn of Co-rich minerals from Katanga (this study –electron microprobe analyses; Burlet et al., 2011; Decrée et al., 2014), New Caledonia (Llorca and Monchoux, 1991), Nkamouna (Dzemua et al., 2013) and Moa Bay (Roqué-Rossell et al., 2010), and bulk lateritic ore in Katanga (Co ore - heterogenite separates, this study), Cerro Matoso (Gleeson et al., 2004), Greenvale (Zeissink, 1969) and Oregon (Hotz, 1964).

Figure 5 UCC-normalized REE patterns for heterogenites of (A) type 1 – Heterogenite separates/Co oxidized ore analyses. REE patterns of Co-sulfides (carrollite from Kamoto, sample RGM 13024 and siegenite from Shinkolobwe, sample GE 3101) are given for comparison purposes, (B) type 2 – Heterogenite separates/Co oxidized ore analyses, (C) type 3 – Heterogenite separates/Co oxidized ore analyses, (D) type 1 – LA-ICP-MS analyses, (E)

type 2 – LA-ICP-MS analyses, the additional pattern shows the difference between RGM 15884 whole rock and LA-ICP-MS analyses, (F) type 3 – LA-ICP-MS analyses, the additional pattern shows the difference between TW015 Heterogenite separates/Co oxidized ore and LA-ICP-MS analyses. UCC values are from McLennan (2001). Grey fields in D, E and F represent the Heterogenite separates/Co oxidized ore analyses.

Figure 6 $Log(Gd/Yb)_{UCC}$ as a function of $log(La/Sm)_{UCC}$ illustrating REE fractionation. Quadrant I corresponds to MREE enriched patterns; quadrant II to LREE enriched patterns and quadrant III to HREE enriched patterns. UCC values are from McLennan (2001). (A) Heterogenite separates/Co oxidized ore analyses and (B) LA-ICP-MS analyses.

Figure 7 Eh-pH stability diagrams at 25°C for (A) Co minerals and dissolved species of Co (system Co-O-H only). Arrow shows heterogenite stability field shift for decreasing Co activity, (B) Mn minerals and dissolved species of Mn (system Mn-O-H only).

Figure 8 Correlation between MnO content and Ce anomaly (A), La_{UCC}/Yb_{UCC} (B), La_{UCC}/Sm_{UCC} (C), Gd_{UCC}/Yb_{UCC} (D), and total REE content (E) within heterogenite (electron microprobe analyses for the MnO contents and LA-ICP-MS analyses for the REE contents).Two trends are observed and emphasized by arrows, see text for further details.

Figure 9 Speciation calculations for (a) La, (b) Eu and (c) Lu in groundwater with [Mn] of 10^{-4} mol/L (d) La, (e) Eu and (f) Lu in groundwater with [Mn] of 10^{-5} mol/L (conditions of groundwater from Wood, 1990). It must be noted that minor F, Cl and P complexes (few % at maximum) are not depicted for clarity.

Figure 10 Sketch diagram illustrating the formation of the different types of heterogenite and their corresponding REE patterns. The latter depend on the environment (subsurface or deeper environment) and on the co-precipitating mineral phases (MnOOH or LREE-enriched carbonate). REE patterns from Katanga Fe-Mn laterites are from Pourret et al. (2014).

Table 1 Location and brief description of the studied heterogenites.

Table

Click here to download Table: Table 1 - REE Heterogenite.docx

Sample	Location	Macroscopic description
Eastern part of the Katanga Copperbelt		
RGM 914	Kiola	heterogenite masses
RGM 924	Kiola	heterogenite geode lining
RGM 3334	Ruashi	impregnation and black layers
RGM 4418	Lwiswishi	earthy and scoriaceous material
DOL1	Luiswishi	crust made up of small botryoids as fissure infillings
RGM 1304	Etoile	finely banded heterogenite
Central part of the Katanga Copperbelt		
RGM 660	Likasi	black mass with malachite crust
RGM 2839	Mindigi	scoriaceous block covered with black botryoids
RGM 12979	Mindigi	nodular heterogenite
RGM 10801	Kalabi	large botryodids
RGM 3335	Kalabi	impregnation
RGM 10807	Kabolela	large botryodids
RGM 12996	Kabolela	botryoidal masses
RGM 13017	Kambove	crust-earthy material
RGM 15884	Kamwali	large botryooidal masses
RGM 10788	Shinko	small botryoids
RGM 10816	Shinko	large botryoids
Western part of the Katanga Copperbelt		
RGM 10805	Musonoi	bright black reniform crust
RGM 10793	Musonoï	massive impregnation of light-coloured schist
RGM 14091	Musonoï	heterogenite impregnation
RGM 13025	Kamoto	heterogenite concretion comprizing silicified-rock clasts (RSC)
RGM 015TW	Tilwezembe	crust-earthy material
RGM 10794	Tilwezembe	crust-earthy material

Figure 1

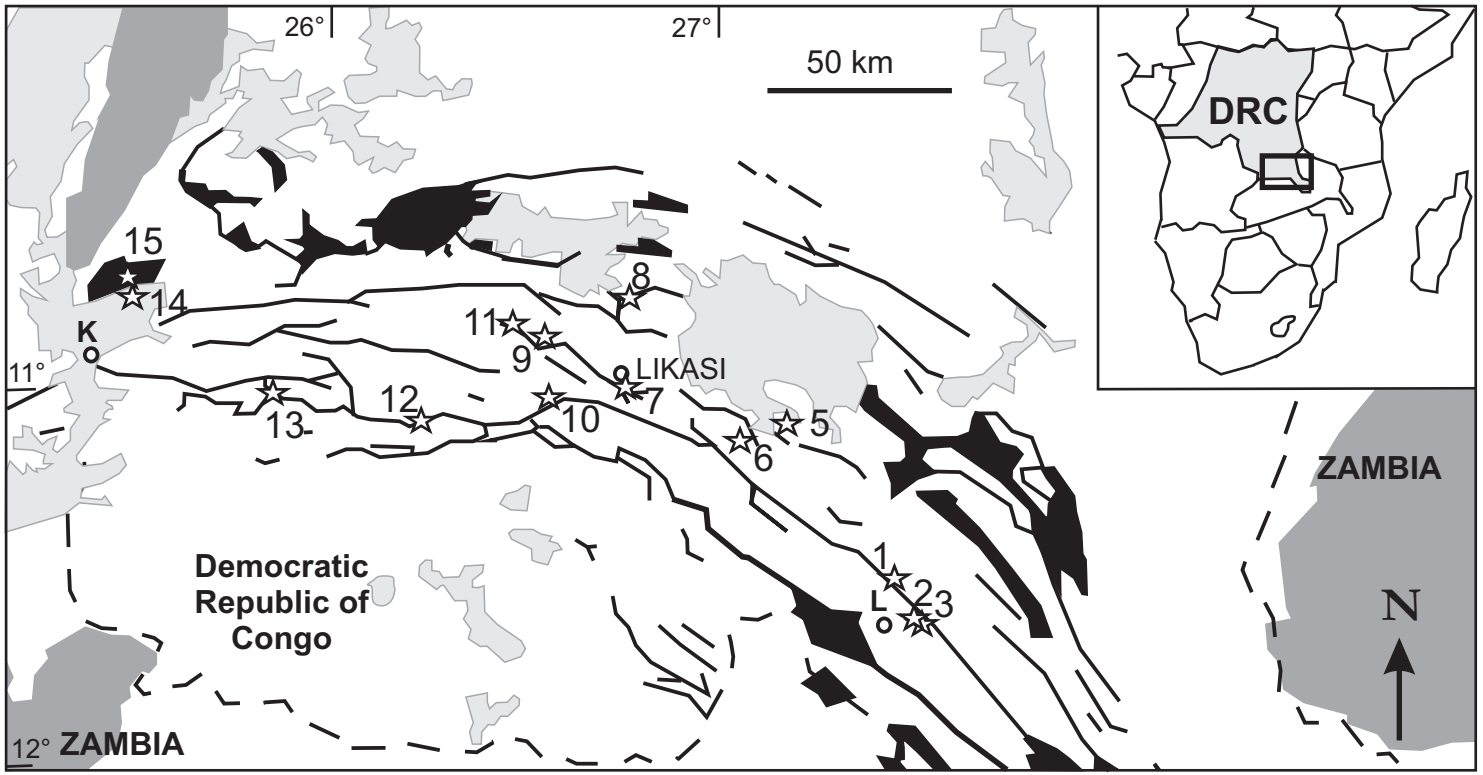

Karoo and Kalahari sediments

R-4, Nguba and Kundelungu rocks

Faults and Roan breccias

Pre-Katangan basement

Town

K. KOLWEZI
L. LUBUMBASHI

☆ Mines from which heterogenites have been sampled

1. Luiswishi
2. Ruashi
3. Etoile
4. Kiola
5. Kamwali
6. Luishia
7. Likasi
8. Kalabi
9. Kambove
10. Shinkolobwe
11. Kabolela
12. Mindigi
13. Tilwezembe
14. Kamoto
15. Musonoi

Figure 2

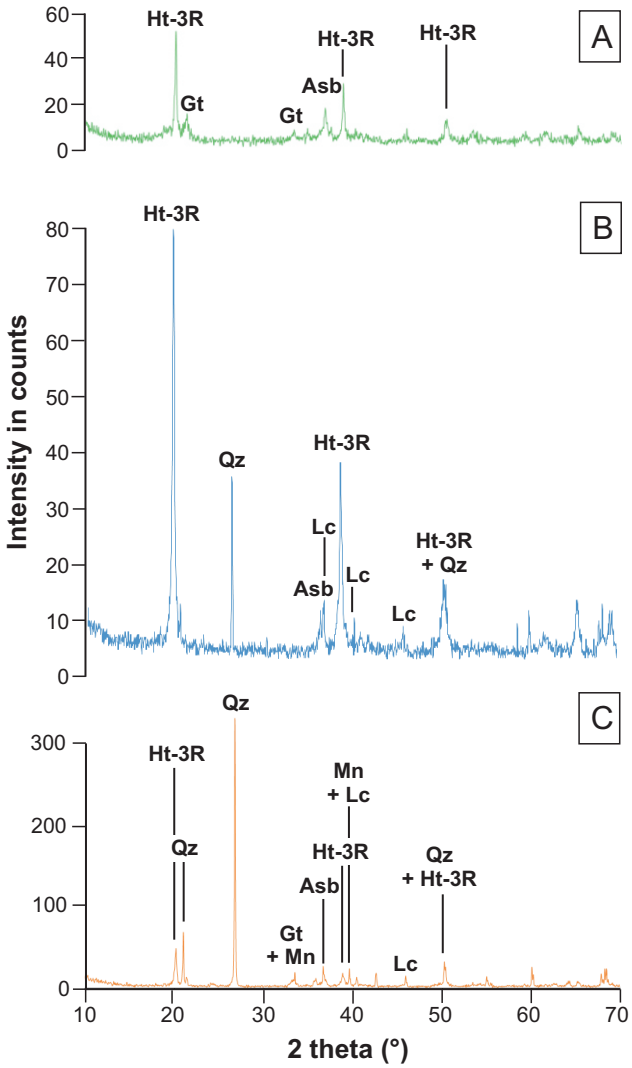
A
Ht-3R
Gt
Gt
Asb
Ht-3R
Ht-3R
B
Ht-3R
Qz
Ht-3R
Lc
Asb
Lc
Lc
Ht-3R
+ Qz
C
Qz
Ht-3R
Qz
Mn
+ Lc
Ht-3R
Asb
Gt
+ Mn
Lc
Qz
+ Ht-3R
Intensity in counts
2 theta (°)

Figure 3

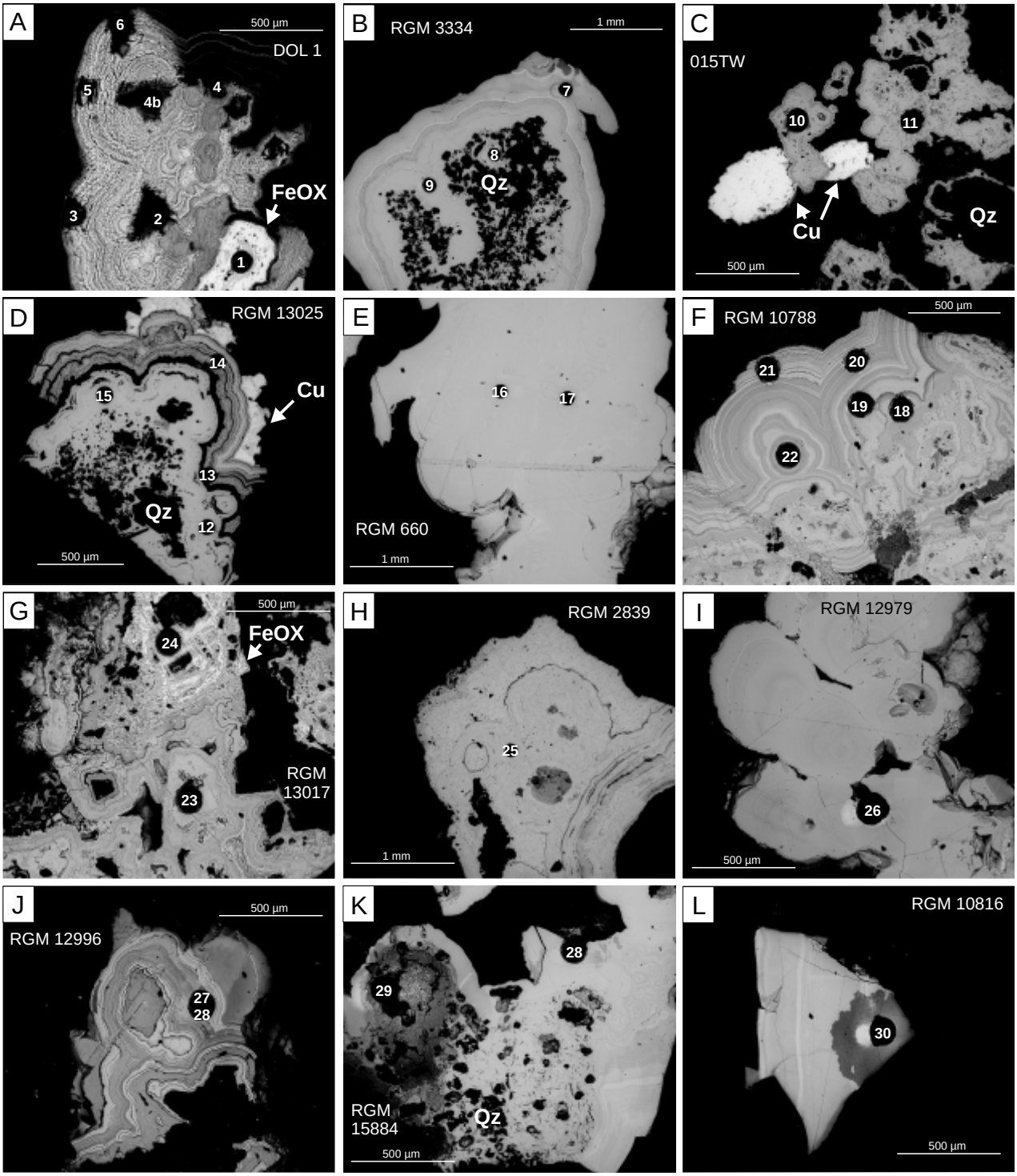
A
500 µm
DOL 1
6
5
4
4b
3
2
1
FeOX
B
RGM 3334
1 mm
7
8
9
Qz
C
015TW
10
11
Cu
Qz
500 µm
D
RGM 13025
14
15
Cu
13
Qz
12
500 µm
E
16
17
RGM 660
1 mm
F
RGM 10788
500 µm
21
20
19
18
22
G
500 µm
24
FeOX
RGM
13017
23
H
RGM 2839
25
1 mm
I
RGM 12979
26
500 µm
J
RGM 12996
500 µm
27
28
K
28
29
RGM
15884
Qz
500 µm
L
RGM 10816
30
500 µm

Figure 4

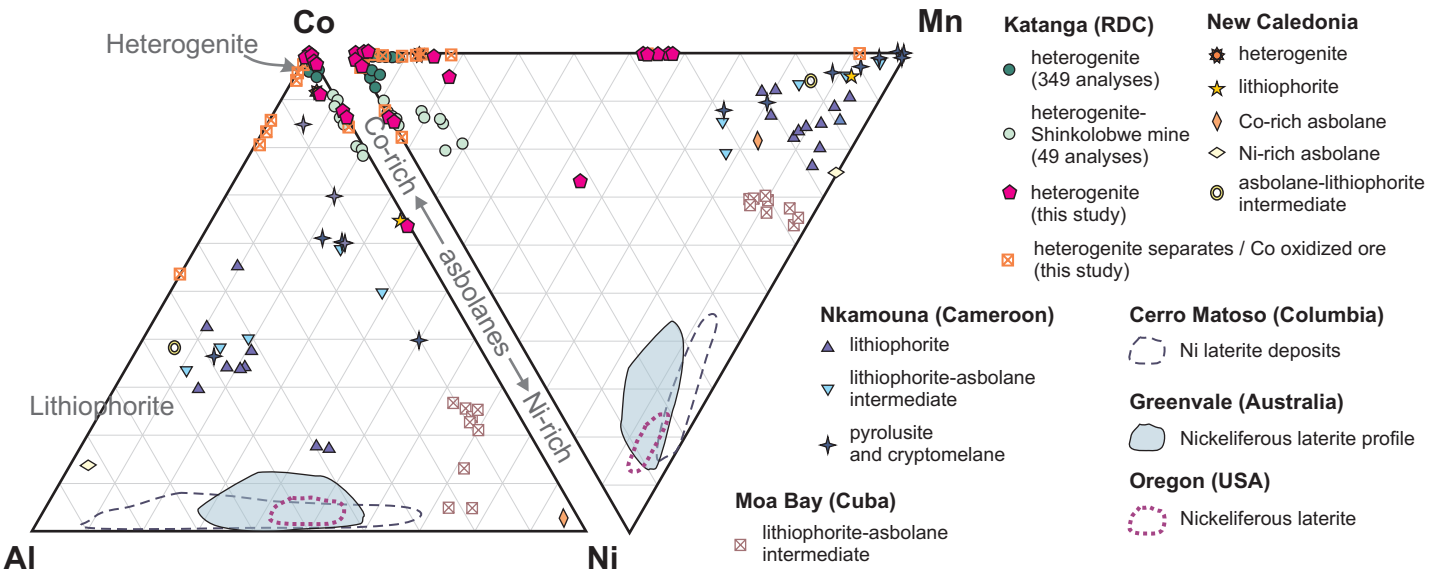
Co
Mn
Al
Ni
Heterogenite
Lithiophorite
Co-rich
asbolanes
Ni-rich
Katanga (RDC)
heterogenite (349 analyses)
heterogenite-Shinkolobwe mine (49 analyses)
heterogenite (this study)
heterogenite separates / Co oxidized ore (this study)
New Caledonia
heterogenite
lithiophorite
Co-rich asbolane
Ni-rich asbolane
asbolane-lithiophorite intermediate
Nkamouna (Cameroon)
lithiophorite
lithiophorite-asbolane intermediate
pyrolusite and cryptomelane
Moa Bay (Cuba)
lithiophorite-asbolane intermediate
Cerro Matoso (Columbia)
Ni laterite deposits
Greenvale (Australia)
Nickeliferous laterite profile
Oregon (USA)
Nickeliferous laterite

Figure 5

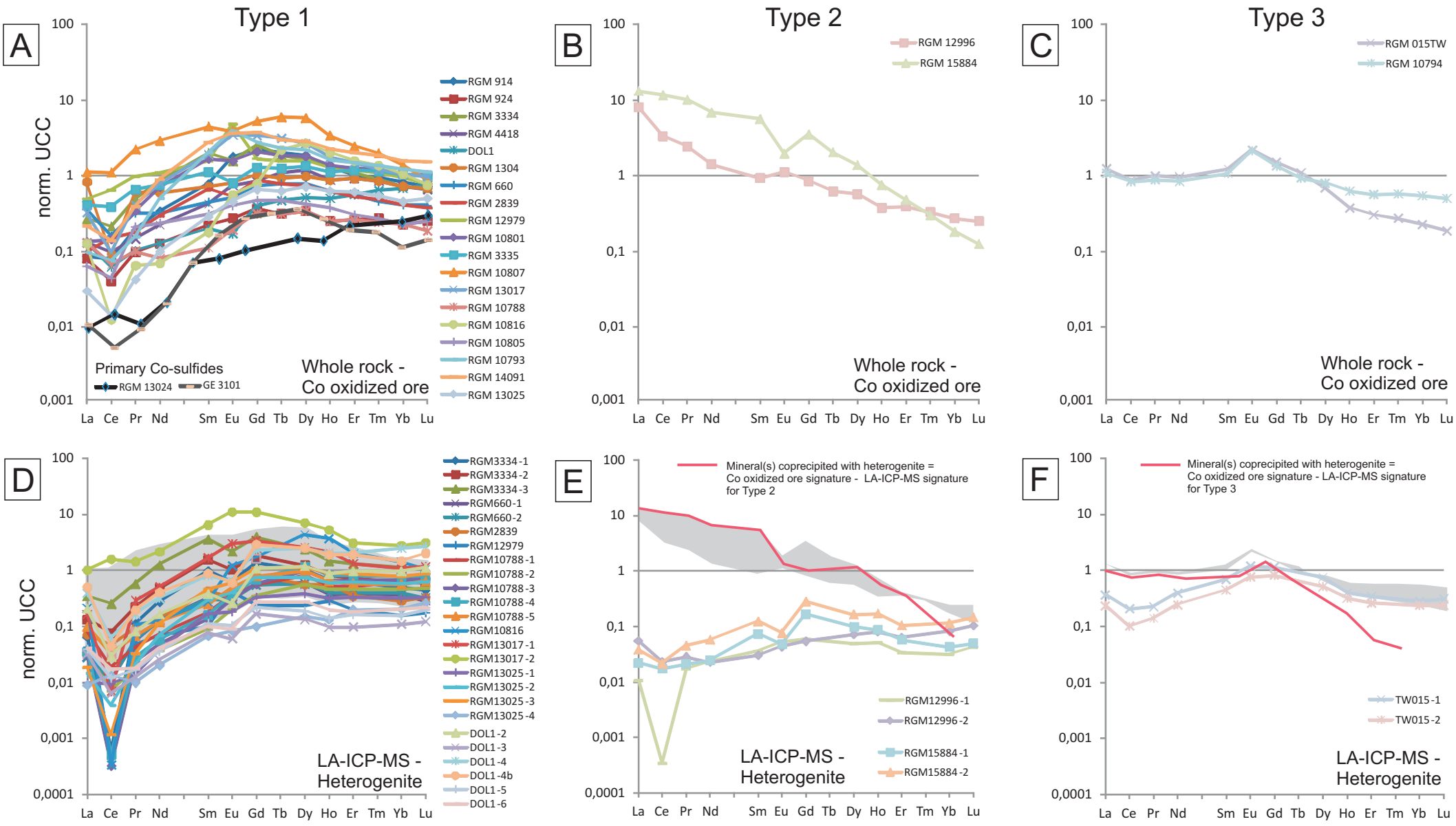
A
Type 1
norm. UCC
100
10
1
0,1
0,01
0,001
La Ce Pr Nd Sm Eu Gd Tb Dy Ho Er Tm Yb Lu
RGM 914
RGM 924
RGM 3334
RGM 4418
DOL1
RGM 1304
RGM 660
RGM 2839
RGM 12979
RGM 10801
RGM 3335
RGM 10807
RGM 13017
RGM 10788
RGM 10816
RGM 10805
RGM 10793
RGM 14091
RGM 13025
Primary Co-sulfides
RGM 13024
GE 3101
Whole rock -
Co oxidized ore
B
Type 2
RGM 12996
RGM 15884
Whole rock -
Co oxidized ore
C
Type 3
RGM 015TW
RGM 10794
Whole rock -
Co oxidized ore
D
norm. UCC
0,0001
RGM3334-1
RGM3334-2
RGM3334-3
RGM660-1
RGM660-2
RGM2839
RGM12979
RGM10788-1
RGM10788-2
RGM10788-3
RGM10788-4
RGM10788-5
RGM10816
RGM13017-1
RGM13017-2
RGM13025-1
RGM13025-2
RGM13025-3
RGM13025-4
DOL1-2
DOL1-3
DOL1-4
DOL1-4b
DOL1-5
DOL1-6
LA-ICP-MS -
Heterogenite
E
Mineral(s) coprecipited with heterogenite =
Co oxidized ore signature - LA-ICP-MS signature
for Type 2
RGM12996-1
RGM12996-2
RGM15884-1
RGM15884-2
LA-ICP-MS -
Heterogenite
F
Mineral(s) coprecipited with heterogenite =
Co oxidized ore signature - LA-ICP-MS signature
for Type 3
TW015-1
TW015-2
LA-ICP-MS -
Heterogenite

Figure 6

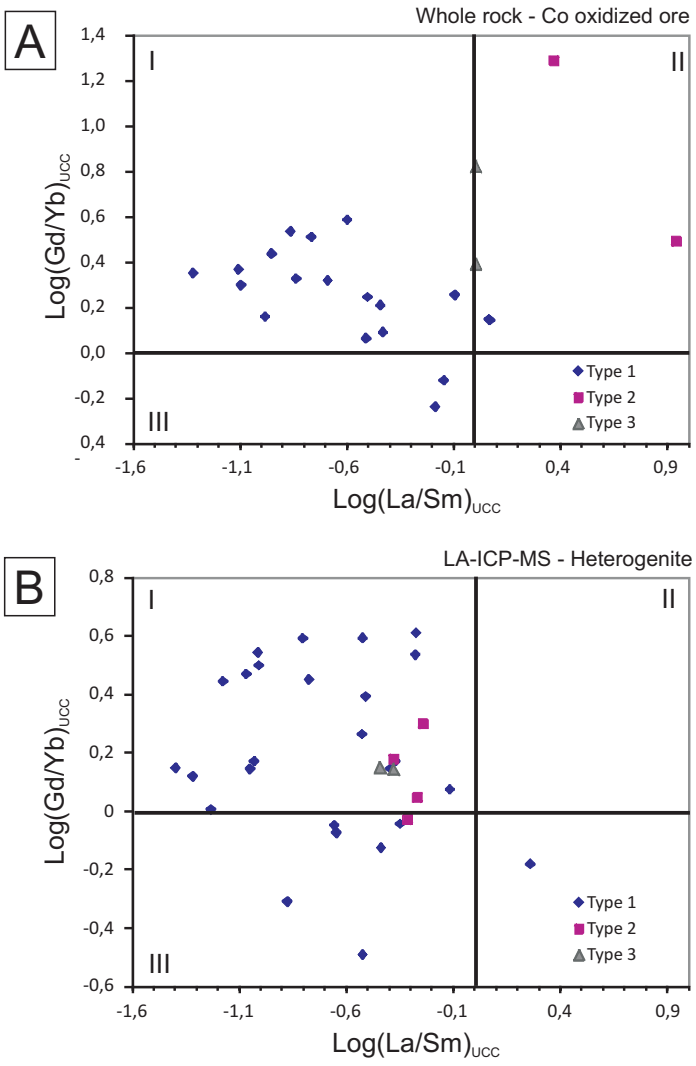
A
Whole rock - Co oxidized ore
I
II
III
Type 1
Type 2
Type 3
Log(Gd/Yb)UCC
Log(La/Sm)UCC
1,4
1,2
1,0
0,8
0,6
0,4
0,2
0,0
-0,2
-0,4
-1,6
-1,1
-0,6
-0,1
0,4
0,9

B
LA-ICP-MS - Heterogenite
I
II
III
Type 1
Type 2
Type 3
Log(Gd/Yb)UCC
Log(La/Sm)UCC
0,8
0,6
0,4
0,2
0
-0,2
-0,4
-0,6
-1,6
-1,1
-0,6
-0,1
0,4
0,9

Figure 7

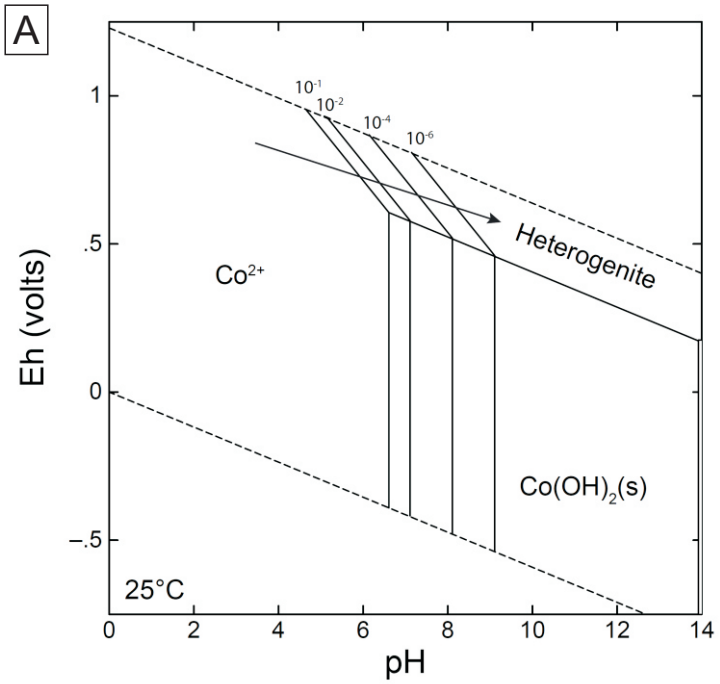
A
10^{-1}
10^{-2}
10^{-4}
10^{-6}
Heterogenite
Co^{2+}
$Co(OH)_2(s)$
25°C
Eh (volts)
pH
1
.5
0
–.5
0
2
4
6
8
10
12
14

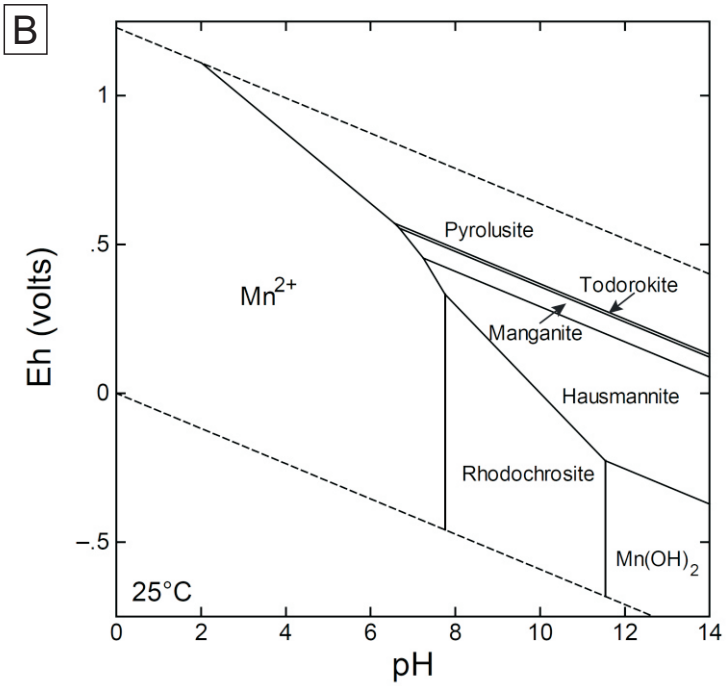
B
Pyrolusite
Todorokite
Manganite
Hausmannite
Rhodochrosite
Mn^{2+}
$Mn(OH)_2$
25°C
Eh (volts)
pH
1
.5
0
–.5
0
2
4
6
8
10
12
14

Figure 8

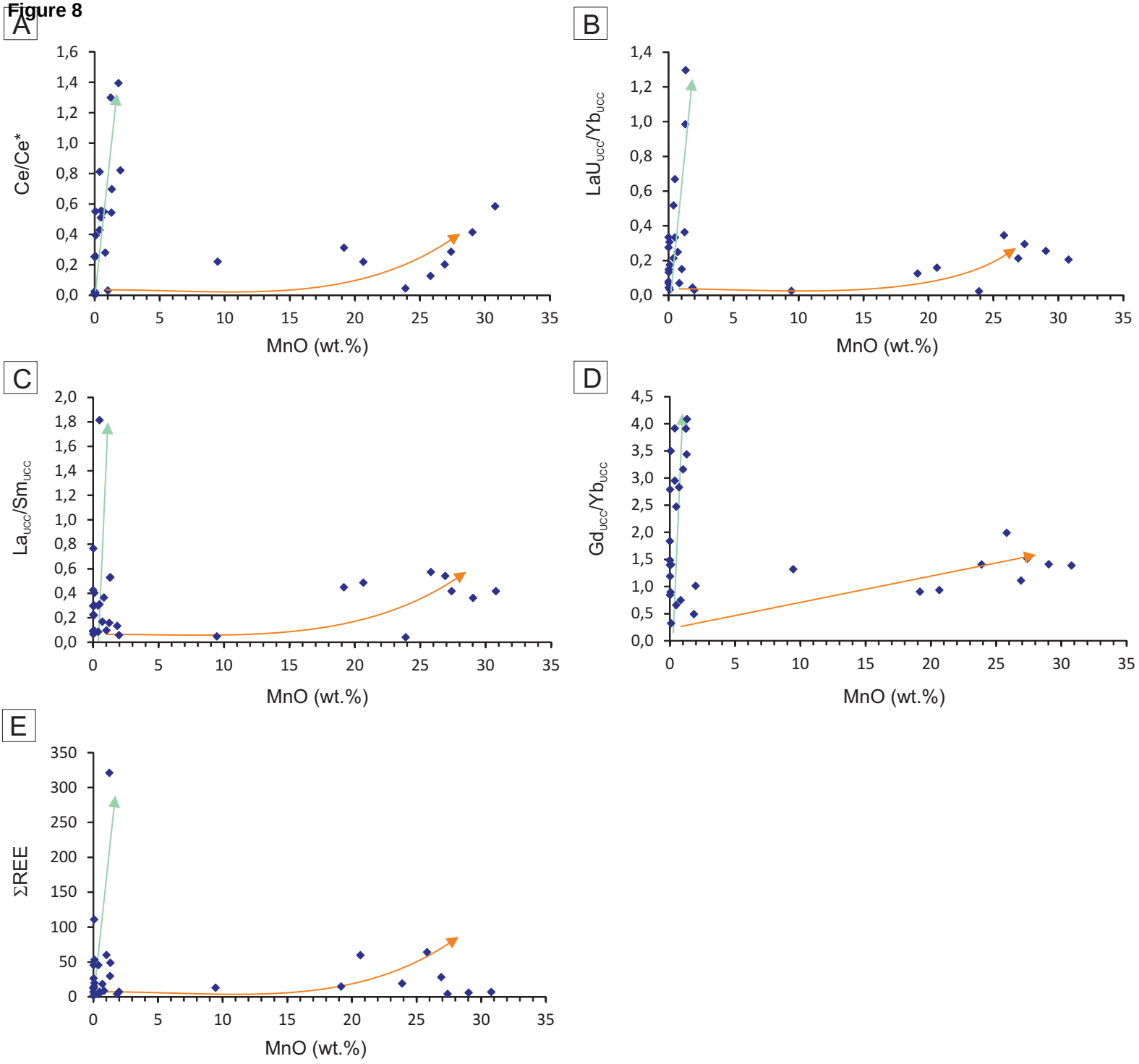
A
Ce/Ce*
MnO (wt.%)
B
LaU$_{UCC}$/Yb$_{UCC}$
MnO (wt.%)
C
La$_{UCC}$/Sm$_{UCC}$
MnO (wt.%)
D
Gd$_{UCC}$/Yb$_{UCC}$
MnO (wt.%)
E
ΣREE
MnO (wt.%)

Figure 9

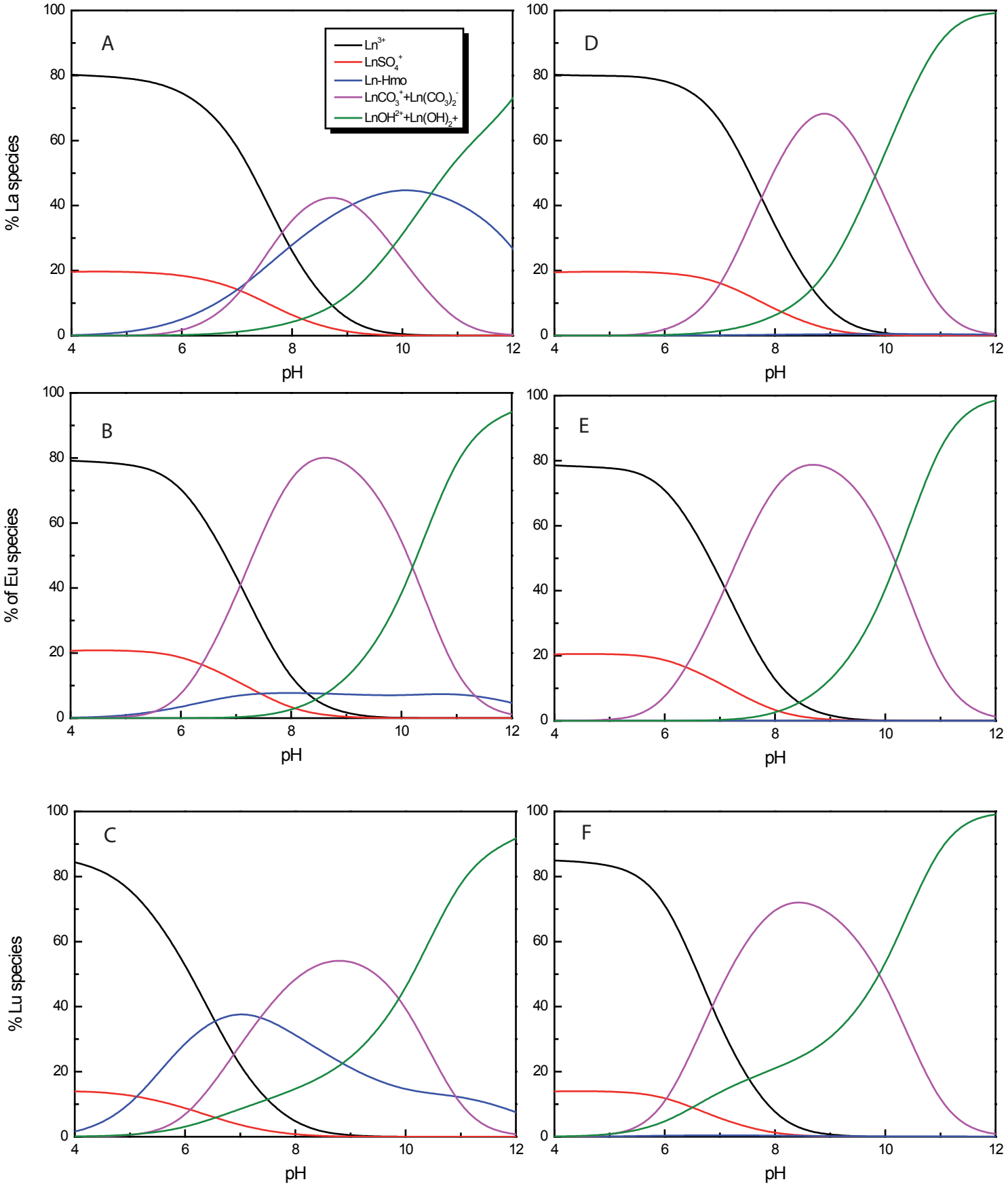
A
B
C
D
E
F
Ln^{3+}
$LnSO_4^+$
Ln-Hmo
$LnCO_3^+ + Ln(CO_3)_2^-$
$LnOH^{2+} + Ln(OH)_2^+$
% La species
% of Eu species
% Lu species
pH
0
20
40
60
80
100
4
6
8
10
12

Figure 10

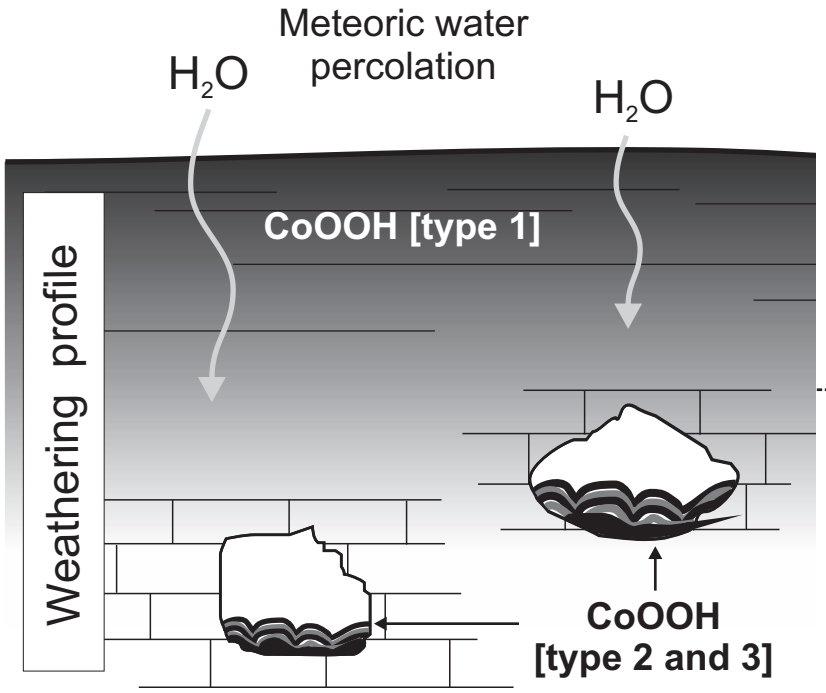

Residual deposit in near-surface environment

→ Heterogenite [1] formation, in association with Mn-oxides

→ Competition for REE

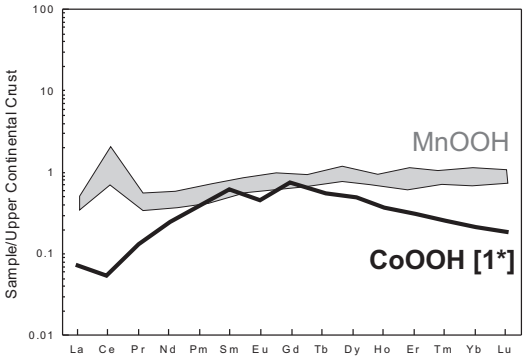

Host-rock (metasediments) dissolution

→ Heterogenite [2 & 3] formation from a carbonate-bearing fluid

→ Probable coprecipitation with a LREE-rich carbonate

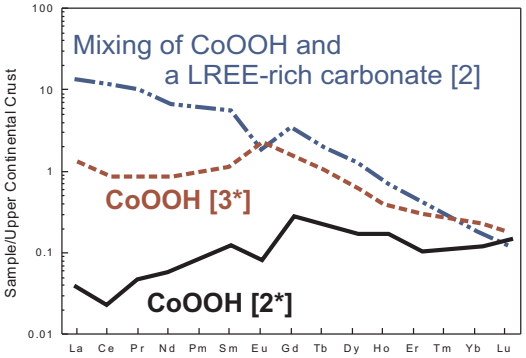

[*] LA-ICP-MS analysis

Authorship Confirmation

Please save a copy of this file, complete and upload as the "Confirmation of Authorship" file.

As corresponding author I, Sophie Decrée, hereby confirm on behalf of all authors that:

1. This manuscript, or a large part of it, has not been published, was not, and is not being submitted to any other journal. If presented at a conference, the conference is identified. If published in conference proceedings, the publication is identified below and substantial justification for re-publication must be presented.

2. All text and graphics, except for those marked with sources, are original works of the authors, and all necessary permissions for publication were secured prior to submission of the manuscript.

3. All authors each made a significant contribution to the research reported and have read and approved the submitted manuscript.

Date February, 18 2015

Previous conference presentation

Goldschmidt 2013 (poster)

Previous conference proceedings publication

Goldschmidt 2013 – Abstract book. P.960

Justification for re-publication